Neither Helix in the Coiled Coil Region of the Axle of F_1-ATPase Plays a Significant Role in Torque Production

Mohammad Delawar Hossain,*† Shou Furuike,* Yasushi Maki,‡ Kengo Adachi,* Toshiharu Suzuki,§¶ Ayako Kohori,* Hiroyasu Itoh,‖** Masasuke Yoshida,§¶ and Kazuhiko Kinosita Jr.*

*Department of Physics, Faculty of Science and Engineering, Waseda University, Shinjuku-Ku, Tokyo 169-8555, Japan; †Department of Physics, School of Physical Sciences, Shahjalal University of Science and Technology, Sylhet 3114, Bangladesh; ‡Department of Physics, Osaka Medical College, Osaka 569-8686, Japan; §Chemical Resources Laboratory, Tokyo Institute of Technology, Yokohama 226-8503, Japan; ¶ATP-Synthesis Regulation Project, International Cooperative Research Project, Japan Science and Technology Agency, Tokyo 135-0064, Japan; ‖Tsukuba Research Laboratory, Hamamatsu Photonics KK, Tokodai, Tsukuba 300-2635, Japan; and **Team 13, Formation of Soft Nano-Machines, Core Research for Evolutional Science and Technology, Tokodai, Tsukuba 300-2635, Japan

ABSTRACT F_1-ATPase is an ATP-driven rotary molecular motor in which the central γ-subunit rotates inside the cylinder made of $\alpha_3\beta_3$ subunits. The amino and carboxy termini of the γ-subunit form the axle, an α-helical coiled coil that deeply penetrates the stator cylinder. We previously truncated the axle step by step, starting with the longer carboxy terminus and then cutting both termini at the same levels, resulting in a slower yet considerably powerful rotation. Here we examine the role of each helix by truncating only the carboxy terminus by 25–40 amino-acid residues. Longer truncation impaired the stability of the motor complex severely: 40 deletions failed to yield rotating the complex. Up to 36 deletions, however, the mutants produced an apparent torque at nearly half of the wild-type torque, independent of truncation length. Time-averaged rotary speeds were low because of load-dependent stumbling at 120° intervals, even with saturating ATP. Comparison with our previous work indicates that half the normal torque is produced at the orifice of the stator. The very tip of the carboxy terminus adds the other half, whereas neither helix in the middle of the axle contributes much to torque generation and the rapid progress of catalysis. None of the residues of the entire axle played a specific decisive role in rotation.

INTRODUCTION

The enzyme ATP synthase consists of a membrane-embedded F_0 portion and an off-membrane F_1 portion (1–3). Both are rotary molecular motors, and are interconnected with each other through a common rotor shaft and a stator stalk (4). A downhill proton flow through the F_0 motor drives rotation of the common shaft, which causes conformational changes in F_1 that lead to the synthesis of ATP from ADP and inorganic phosphate (P_i). Conversely, hydrolysis of ATP in F_1 can make the rotor rotate in the reverse direction, so that F_0 is forced to pump protons in the reverse direction (against the proton gradient). The proton flow in F_0 is thus coupled with the chemical reaction (ATP synthesis/hydrolysis) in F_1 by a rotational catalysis mechanism (5,6). The isolated F_1 motor only hydrolyzes ATP, and is called F_1-ATPase. The minimal subcomplex of F_1-ATPase capable of ATP hydrolysis-driven rotation consists of $\alpha_3\beta_3\gamma$ subunits (4,7), which we here refer to also as F_1. In a crystal structure of mitochondrial F_1 (MF_1; see Fig. 1), the central γ-subunit is surrounded by the stator cylinder formed of $\alpha_3\beta_3$ subunits (8). Three catalytic nucleotide-binding sites reside at β-α interfaces, and are hosted primarily by a β-subunit. In the original structure (8), the three sites contain an ATP analog (between β_{TP} and α_{TP}), ADP (β_{DP} and α_{DP}), and no nucleotide (β_E and α_E). The other three interfaces form, mainly through an α-subunit, noncatalytic nucleotide-binding sites, which bind the ATP analog in the crystal. The noncatalytic sites take part in relieving the enzyme of the MgADP-inhibited state (9–11).

During ATP hydrolysis, the central γ-subunit rotates in the counterclockwise direction when viewed from the F_0 side (12), in steps of 120° per ATP hydrolyzed (13,14). The 120° step is divided into 80–90° and 40–30° substeps, separated by at least two chemical reactions, each taking ~1 ms at room temperature. The 80–90° substep is driven by ATP binding and likely also by ADP release, and the 40–30° substep by the release of P_i (15,16). Hydrolysis of ATP occurs in the 80–90° interim (17). The $\alpha_3\beta_3$ hexamer of F_1 from thermophilic *Bacillus* PS3 (TF_1) has a structure similar to MF_1, but is threefold symmetric in the absence of bound nucleotides (18). It is the asymmetric γ-subunit that dictates which of the three basically equivalent catalytic sites will bind an ATP molecule (19). Dictation by the γ-subunit was clearly demonstrated in an experiment (20) where clockwise rotation of the γ-subunit, driven by an external force, led to ATP synthesis in the catalytic sites of the $\alpha_3\beta_3\gamma$ subcomplex of TF_1: by itself, F_1 is a reversible mechano-chemical energy converter in which the γ-angle determines which of the chemical reactions (binding/release of ADP and P_i, synthesis/hydrolysis

Submitted June 15, 2008, and accepted for publication August 5, 2008.

Address reprint requests to Kazuhiko Kinosita Jr., Dept. of Physics, Faculty of Science and Engineering, Waseda University, 3-4-1 Okubo, Shinjuku-Ku, Tokyo 169-8555, Japan. Tel.: 81-3-5952-5871; Fax: 81-3- 5952-5877; E-mail: kazuhiko@waseda.jp.

Editor: David D. Hackney.

0006-3495/08/11/4837/08 $2.00

doi: 10.1529/biophysj.108.140061

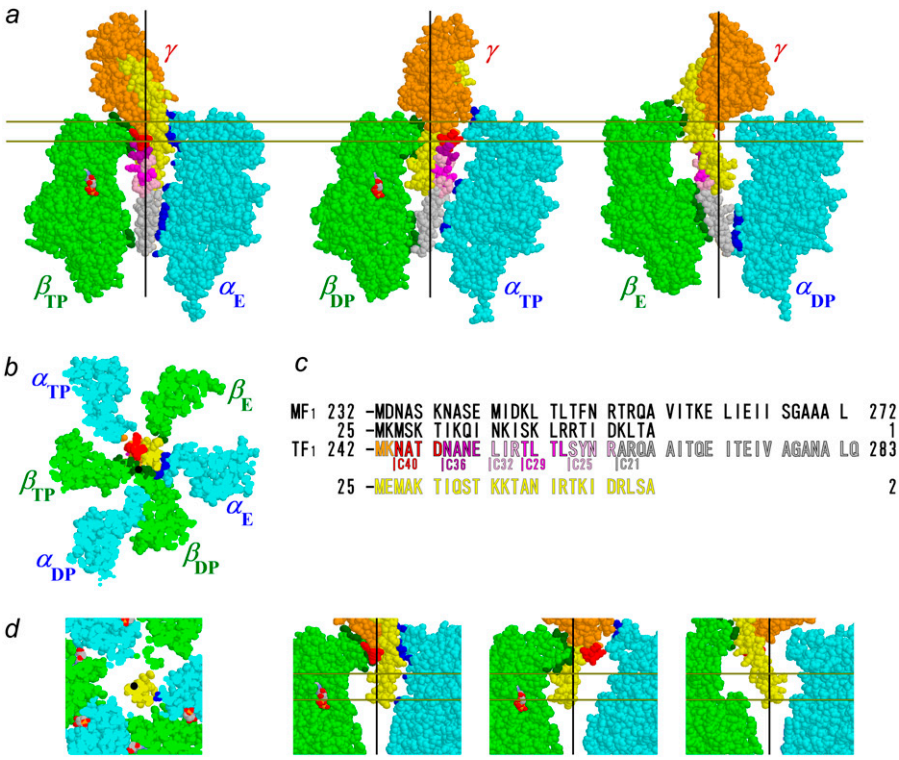

FIGURE 1 Atomic structure of MF_1 (22). Truncations of γ-subunit are shown, with color scheme in *c*; the N-terminal α-helix is shown in yellow. Those atoms of α-subunits and β-subunits that are within 0.5 nm from an atom of γ (excluding hydrogens) are colored blue and dark green, respectively. Nucleotides are shown in CPK colors. Black lines in side views and black dots in bottom views represent putative rotation axis (21). (*a*) Side views show central γ and an opposing α-β pair. Membrane-embedded F_0 portion of ATP synthase would be above the γ-subunit. (*b*) Bottom view of section between pair of gold lines in *a*. (*c*) Amino-acid sequences at the C-terminus and N-terminus of γ in MF_1 (36) and TF_1 (30), except that numbering for TF_1 in our study here starts from Met-1, which is absent in the expressed wild-type protein. In Fig. 1 *B* of Furuike et al. (27), Ala-2 was incorrectly shown as Ala-1. (*d*) Central portions of bottom and side views for γ-ΔC36.

of ATP, and release/binding of ATP) will occur in the three catalytic sites.

Although the basic coupling scheme between rotation and chemical reactions was worked out (16) as outlined above, the structural basis of torque generation remains unclear. One suggestion involved a push-pull mechanism (21). In the MF_1 structure in Fig.1 *a* (22), the axle of the F_1 motor, i.e., the portion of the γ-subunit that deeply penetrates the $\alpha_3\beta_3$ cylinder, is formed of the antiparallel α-helical coiled coil of amino- (N-) and carboxy- (C-) termini, the bottom tip comprising the longer C-terminal α-helix alone. The axle is held by the stator cylinder at two positions, i.e., the top orifice and the bottom (Fig. 1, *dark green* and *blue atoms*). The β-subunits binding a nucleotide (β_{TP} and β_{DP}) are bent toward, and apparently push, the axle at the top, whereas the empty β-subunit (β_E) retracts and pulls the axle. The push-pull actions would rotate the skewed and slightly curved axle in a conical fashion. This mechanism would require the axle to be rigid and its tip be held relatively stationary as a pivot. Indeed, the bottom of the $\alpha_3\beta_3$ cylinder forms a hydrophobic ''sleeve'' that could act as a bearing (8). For communication of the γ-angle to the catalytic sites, the lever action of a rigid axle would also be an efficient mechanism.

Truncation of the axle will reveal whether, or to what extent, the rotation and control of catalysis rely on the pivoting of a rigid axle. In earlier studies, a deletion of 10 residues (23) at the C-terminus of *Escherichia coli* F_1 (EF_1) or of 20 C-terminal residues (24) of chloroplast F_1 (CF_1) resulted in reduced but significant ATPase activity. With a deletion of 12 C-terminal residues, EF_1 remained functional, without affecting torque, although hydrolysis activity was gradually diminished at longer deletions (25). We truncated the C-terminus of TF_1-γ up to 21 residues (Fig. 1 *a*, *gray*), but the mutants rotated with a torque ~50% or more of the wild-type (26). These studies did not remove the bottom interactions completely: the remaining axle tip would still touch the bottom sleeve of the stator cylinder. In our most recent study (27), we found that an axle-less mutant in which 43 C-terminal and 22 N-terminal residues of the γ-subunit of TF_1 were deleted (up to slightly above the red residues and opposing yellow residues in Fig. 1 *a*) still rotated in the correct direction. This work ruled out the necessity of pivoting action of a rigid axle in producing unidirectional rotation. However, both the rotary speed and the rate of ATP hydrolysis decreased as we truncated the axle (opposing N-terminal and C-terminal α-helices were truncated simultaneously, such that their remaining tips were at about the same height), and short mutants could rotate only small (40 nm in diameter) beads and not larger ones (0.29 μm and above). Efficient catalysis would still require axle-stator interactions.

Here, we investigated the role of the C-terminal α-helix of the γ-subunit by truncating it stepwise beyond 21 amino-acid residues, leaving the N-terminal helix intact in the stator cavity. Mutants of up to 36 deletions were active with reduced functionality, although their stability gradually decreased with longer deletions. The 36-deletion mutant, in which the entire C-terminal α-helix inside the stator cavity was absent, rotated stepwise with ~50% the torque of the wild-type. The very tip of the C-terminal α-helix that touches the bottom sleeve is essential for rapid catalysis and generation

of full torque, but the rest of the C-terminal helix up to the base of the axle is completely unnecessary for the residual rotation with half the torque. The N-terminal helix also contributes little, in that its presence does not improve rotational characteristics significantly.

MATERIALS AND METHODS

Streptavidin-coated polystyrene beads (0.29 μm in diameter) were purchased from Seradyn (Indianapolis, IN). Biotin-$PEAC_5$-maleimide was from Dojindo (Kumamoto, Japan), and other chemicals were of the highest grade commercially available. In rotation and hydrolysis experiments, Mg^{2+} was always 2 mM in excess over ATP.

Construction of mutants

Mutations were constructed on the plasmid pKABG1/HC95 that carries genes for the α (C193S), β (His_{10} at the amino terminus), and γ (S107C and I210C) subunits of TF_1 that we regard as the wild-type (15,28). We introduced γ C-terminal truncations, designated as γ-ΔC*m*, where *m* is the number of residues deleted, in pKABG1/HC95, as previously described (26,27). The mutations were confirmed by DNA sequencing (Shimadzu Biotech, DNA Sequence Service, Kyoto, Japan). In *E. coli* strain JM103 Δ(uncB–uncD), which has lost the ability to express authentic F_oF_1-ATPase (29), all mutant proteins were expressed to a level similar to that of the wild-type. Purified γ-ΔC36 was checked by MALDI-TOF mass spectrometry (APRO Life Science Institute, Naruto, Japan). The γ-ΔC36 contained three major components with masses of 54,700 (expected mass for α, 54,714.8), 53,340 (expected mass for β, 53,355.9), and 27,770 (expected mass for γ Ala-2 to Asp-247, 27,785.1). The amino-acid sequence here and in Fig. 1 *c* is from Ohta et al. (30), except that our numbering in this and in previous work (26,27) began with Met-1, which is absent in the expressed wild-type, and which we assume is also absent in the mutants described here. The actual sequence of TF_1 that we used here and previously (26,27) is slightly different from that in Ohta et al. (30), and the C-terminus of the wild-type in this study is Gln-285 and not Gln-283, counting from Met-1 (M. Yoshida, unpublished findings). Because the differences are not in the N-terminal and C-terminal that form the axle, we adopt the published sequence in this study. The expected masses above, however, were calculated on the basis of the actual sequence.

Purification and biotinylation of F_1

Wild-type and mutant F_1 were purified as described (26,27,31), without heat treatment and passage through a butyl-Toyopearl column (Tosoh 650M, Tokyo, Japan, used for removal of bound nucleotide). The cell lysate was ultracentrifuged for 30 min at 40,000 rpm. Decanted supernatant was passed through a Ni^{2+}-nitrilotriacetic acid (Ni-NTA) Superflow column (Qiagen, Hilden, Germany). The eluent containing F_1 in buffer A (300 mM imidazole, pH 7.0, and 100 mM NaCl) was mixed with 70% ammonium sulfate and 2 mM dithiothreitol (DTT), and stored at 4°C. Before use, the precipitate was dissolved in buffer B (100 mM KP_i, pH 7.0, and 2 mM EDTA) and passed through a size exclusion column (Superdex 200 HR 10/30, Amersham Pharmacia, Piscataway, NJ) pre-equilibrated with buffer B to remove DTT and possible denatured enzyme. All procedures were at 4°C, except for the Ni-NTA column treatment, which was at room temperature.

Purified F_1 was biotinylated at the two cysteines (γ-107C and γ-210C) by incubation with a fourfold molar excess of biotin-$PEAC_5$-maleimide within 4 h after lysis of *E. coli*. Unbound biotin was removed using the above size exclusion column, pre-equilibrated with buffer B.

Measurement of hydrolysis activity

The rate of ATP hydrolysis by the mutants at 2 mM ATP was measured using a spectrophotometer (model U-3100, Hitachi, Tokyo, Japan) at 23°C. The reaction was started by rapidly adding unbiotinylated F_1 in buffer B, at a final concentration of 5–10 nM, into buffer C (10 mM MOPS (3-(*N*-morpholino)propanesulfonic acid)-KOH, pH 7.0, 50 mM KCl, and 2 mM $MgCl_2$) containing an ATP regeneration system consisting of 0.2 mM NADH (nicotinamide adenine dinucleotide), 1 mM phosphoenolpyruvate, 250 μg mL^{-1} pyruvate kinase (rabbit muscle, Roche Diagnostics, Mannheim, Germany), and 50 μg mL^{-1} lactate dehydrogenase (hog muscle, Roche Diagnostics). The hydrolysis rate was determined from the decrease in NADH absorbance at 340 nm (10). The rate was estimated over 2–40 s after mixing.

Preparation of Ni-NTA glass surface

Glass coverslips (NEO Micro Cover Glass No. 1, 24 × 32 mm^2, Matsunami, Osaka, Japan) were set vertically and separately on a ceramic glass holder, and were immersed in 12 N KOH for 24 h to clean the surfaces (20,26). Then the coverslips, along with the holder, were extensively washed with ultrapure water. To 100 mL ultrapure water in a glass beaker containing a small stirrer bar, 0.02% (v/v) acetic acid was added and mixed well on a magnetic stirrer at 60°C in a fume hood; ~2% (v/v) 3-mercaptopropyltrimethoxysilane (TSL8380, Toshiba GE silicone, Toshiba, Tokyo, Japan) was then added with a glass pipette and mixed. The prewashed coverslips in the holder were placed carefully in the silane solution, and stirring continued for a further 15–20 min. The hot glass beaker containing the silane solution and coverslips was taken out of the fume hood and placed in a constant-temperature oven at 90°C for 2 h. After cooling in the fume hood, the coverslips were washed vigorously with ultrapure water. On a clean paper, 20 μL of 100 mM DTT in 10 mM MOPS-KOH, pH 7.0, were sandwiched between pairs of silanized coverslips and kept for 20 min at room temperature to reduce the −SH groups on the surfaces. After vigorous washing with ultrapure water, 10 mg mL^{-1} Maleimide-C_3-NTA (Dojindo) in 10 mM MOPS-KOH, pH 7.0, was sandwiched between coverslip pairs and incubated for 30 min at room temperature. After washing with water, the coverslips were incubated at room temperature in 100 mL of 10 mM $NiCl_2$ for 20 min. Finally, the coverslips in the holder were washed and stored in 100 mL of ultrapure water at room temperature. They were used within a few weeks.

Observation of rotation

A flow chamber was constructed of the Ni-NTA-coated bottom coverslip (24 × 32 mm^2) and a top uncoated coverslip (18 × 18 mm^2), separated by two greased strips of Parafilm cover sheet. Rotation assays were conducted in buffer C containing an ATP regenerating system consisting of 0.2 mg mL^{-1} creatine kinase (rabbit muscle, Roche Diagnostics) and 2.5 mM creatine phosphate (Roche Diagnostics). Streptavidin-coated beads of 0.29-μm diameter were washed three times with buffer C containing 5 mg mL^{-1} bovine serum albumin (BSA; Fluka, Buchs, Switzerland) through centrifugation at 15,000 rpm for 10 min at 4°C to remove preservatives. The concentration of beads was finally adjusted to 0.1% (w/v) with 5 mg mL^{-1} BSA. One flow-chamber volume of biotinylated 0.5–100 nM F_1 was infused into the chamber and incubated at room temperature for 2 min, so that the F_1 subcomplex was fixed on the Ni-NTA coated coverslip through the histidine tags. The chamber was then washed three times with 5 mg mL^{-1} BSA and incubated for 5 min. One chamber volume of the prewashed streptavidin-coated beads was infused into the chamber and kept for 15 min at room temperature, so that beads were attached to the biotinylated γ-subunit of the $\alpha_3\beta_3\gamma$ complex. The flow cell was washed three times with buffer C to remove unbound beads. Finally, five chamber volumes of 2 mM MgATP in buffer C containing the regeneration system were infused, and the chamber was sealed with silicone grease to avoid evaporation. Rotation was observed at 23°C on an inverted microscope (IX71, Olympus, Tokyo, Japan) with a stable mechanical stage (KS-O, ChuukoushaSeisakujo, Tokyo, Japan). Bead images were captured with a CCD camera (Lynx IPX-VGA210L, Imperx, Boca Raton, FL) at 500 frames s^{-1} as an eight-bit AVI file. The centroid of bead images was calculated as described previously (15). For clear identification of rotation, a duplex of beads was always selected for analysis.

Estimation of torque

The torque N that the motor produced was estimated from the instantaneous rotary speed ω (in radian s^{-1}) during a 120° step, using (13,32):

$$N = \omega\xi, \tag{1}$$

where ξ is the frictional drag coefficient given, for the case of a duplex of spherical beads, by

$$\xi = 2 \times 8\pi\eta a^3 + 6\pi\eta a x_1^2 + 6\pi\eta a x_2^2, \tag{2}$$

where a is the bead radius, x_1 and x_2 the radii of the rotation of inner and outer beads, and η is the viscosity of the medium ($\sim 0.93 \times 10^{-3}$ N s m^{-2} at 23°C). We selected those duplexes with $x_2 > 0.2$ μm; x_1 was taken as 0. The drag in Eq. 2 is likely an underestimate (13,33).

RESULTS

Assembly of mutant subcomplexes

In this study, we used an $\alpha(C193S)_3\beta(His_{10}$ at amino terminus$)_3\gamma$(S107C, I210C) subcomplex of TF_1 (15) as the wild-type. This subcomplex has sole two cysteines at the protruding portion of the γ-subunit for labeling with an external probe, and histidine tags at the bottom of the β- subunits for attachment of the protein to a glass surface. We made mutants in which 25, 29, 32, 36, or 40 amino-acid residues were deleted from the C-terminus of the γ-subunit, i.e., γ-ΔC25 to γ-ΔC40. All these mutants were expressed in *E. coli* to a level similar to that of the wild-type. In particular, the expression level of the γ-subunit was independent of the degree of truncation. The yield of purified mutant subcomplex containing the γ-subunit, however, was variable and lower compared with the wild-type (Fig. 2): short mutants did not assemble well. We also found that shorter mutants were unstable upon storage, and we had to use γ-ΔC32 and γ-ΔC36 within 3 days of final purification.

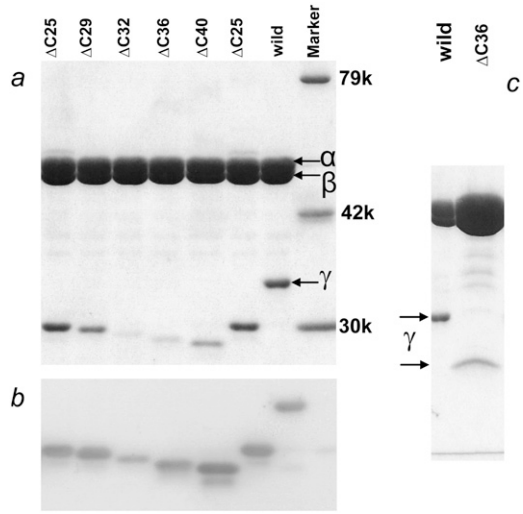

FIGURE 2 Confirmation of γ-truncations by polyacrylamide gel electrophoresis. (*a*) Ten percent gel contains 0.1% SDS, stained with Coomassie brilliant Blue R-250. (*b*) Western blot of *a* stained with anti-γ-antibody. (*c*) Overloaded gel shows absence of intact γ in mutant. Amount of γ in purified samples was variable, depending on preparations; γ-ΔC40 in another preparation showed a barely detectable γ band. Side bands in *b* are presumably dissociated and degraded γ.

Rotation

Rotation of the wild-type and mutants was observed by attaching the β-subunits to a glass surface through the histidine residues at the N-terminus, and putting a duplex of 0.29-μm beads on the γ-subunit as a marker. We found rotary beads up to γ-ΔC36, but none with γ-ΔC40. When a duplex on a mutant rotated, it did so in a counterclockwise direction, as with the wild-type (observed from above in Fig. 1 *a*), usually for more than 100 revolutions, even with γ-ΔC36 (Fig. 3 *a*).

Finding rotary beads became progressively difficult for shorter mutants. With the wild-type, several hundred rotating bead duplexes were found per observation chamber when F_1 at 0.5 nM was infused. Mutants were examined within 3–4 days of preparation (kept at room temperature because TF_1 is cold-labile), and F_1 at a higher concentration had to be applied to observe rotation. With γ-ΔC25, 20–25 duplexes rotated per chamber at 2 nM F_1; 8–10 duplexes at 10 nM γ-ΔC29; 3–4 duplexes at 20 nM γ-ΔC32; and ~2 duplexes at 50 nM γ-ΔC36, if observed within 2 days (none rotated after 4 days). Rotation could be observed for at least 2 h after chamber preparation. Nonrotating mutant γ-ΔC40 was closely examined in 5–6 chambers at various F_1 concentrations up to 100 nM, beginning a few hours after purification, but no bead rotated.

Rotation time courses of beads that rotated relatively fast at 2 mM ATP are shown in Fig. 3. For mutants except γ-ΔC25, we failed to observe rotation at lower ATP concentrations. Rotation of wild-type F_1 was basically continuous at a video resolution of 2 ms. At this saturating ATP concentration, a catalytic cycle of ATP hydrolysis under unloaded conditions takes only ~2 ms at room temperature (15), and thus the average speed of ~15 revolutions per second (rps) observed here is limited by viscous friction against the 0.29-μm bead duplex. Time-averaged speeds of mutants were an order of magnitude lower, ranging from ~2 rps (γ-ΔC25) to ~0.5 rps (γ-ΔC36). The cause is not the mutants' lower torque, which would result in a lower speed at all moments, but the mutants' tendency to dwell at angles separated by 120° (Fig. 3 *b*). Unlike longer mutants in our previous study (γ-ΔC21 or longer) (26), we could not find rotation when 0.49-μm beads were attached instead of the 0.29-μm beads. The failure to find rotation in γ-ΔC40 with 0.29-μm beads, despite the rotation, though very rare, of 40-nm beads attached to γ-ΔN22C43 (27), also points to a load effect.

The wild-type also showed a tendency to stumble at angles separated by 120°, even at 2 mM ATP, at ~80° ahead of ATP-waiting angles (32). The stumbling in the wild-type is load-dependent: with a high load such as a duplex of 0.95-μm beads, we often observed a momentary pause at this angle, but pauses were less conspicuous with smaller beads. At this

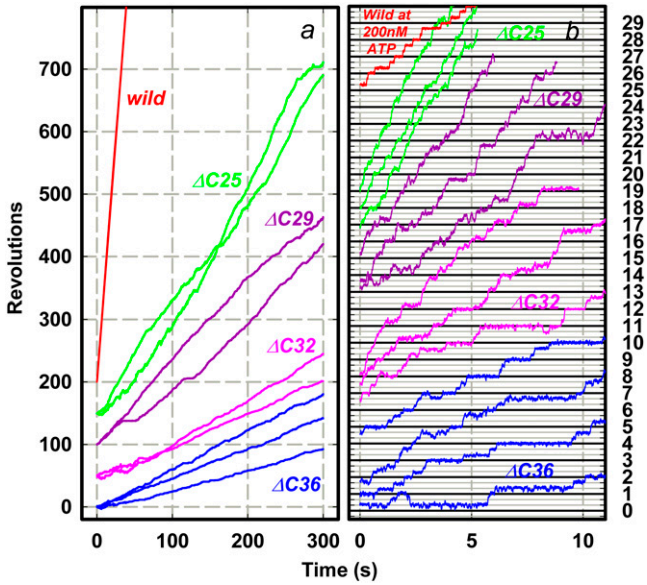

FIGURE 3 Time courses of rotation of 0.29-μm bead duplex attached to γ-subunit. All rotations were counterclockwise when viewed from above in Fig. 1 *a*. Horizontal lines in *b* are separated by 120°. ATP concentration was 2 mM, except for the wild-type in *b*, which stepped because of infrequent binding of ATP at 200 nM (rate constant for ATP binding (13), $\sim 2 \times 10^7$ $M^{-1}s^{-1}$). Dwelling angles of mutants are plotted ~80° ahead of ATP-waiting dwells of the wild-type, because long pauses such as those in γ-ΔC29 in *a* also occurred at same angles and because long pauses in the wild-type, because of MgADP inhibition (11), occur at ~80°. This assignment, however, is tentative because we could not determine ATP-waiting angles of mutants. Bottom curve in *b* shows an exceptional case of reversal over two 120°-steps in a sluggish phase, after which more regular rotation resumed beyond the right-hand axis. Temperature, 23°C.

angle, the torque of the motor vanishes until the splitting of ATP into ADP and P_i and the release of P_i have taken place, each requiring ~1 ms under a negligible load (7,15–17). Presumably, a thermal barrier against one or both of these reactions is effectively heightened by friction between the beads and the glass surface (or between the beads and F_1), leading to a longer dwell before torque generation. The implication here is that climbing the barrier requires some rotation or rotational fluctuation, as, for example, discussed for P_i release (16). For the mutants, we could not ascertain the angles of stumbling, but the load dependence suggests that the mutants also tend to dwell at ~80° ahead of ATP-waiting angles. The barrier at these angles would be higher for the mutants because of inefficient coupling between γ rotation and chemical reactions, or because fluctuation (inclination) of short γ may increase the chance of surface interaction. Possibilities other than the barrier at ~80° cannot be excluded.

ATP hydrolysis activity

The rate of ATP hydrolysis measured under bulk, unloaded conditions supported the above view that load-dependent stumbling slows down the rotation. Precise estimation of the rate of hydrolysis was impossible, because mutant γ tended to dissociate from the subcomplex, and for this reason, we were unable to go through the time-consuming procedure of removing completely the tightly bound inhibitory nucleotide (31). Without correcting for these effects, and thus at lower bounds, we obtained the following hydrolysis rates (Fig. 4 *b*): ~22 s^{-1} (γ-ΔC25), ~16 s^{-1} (γ-ΔC29), ~9 s^{-1} (γ-ΔC32), and ~8 s^{-1} (γ-ΔC36) at 2 mM ATP, which we confirmed as saturating (same rates at 6 mM ATP). These values are lower than the wild-type rate of ~300 s^{-1} (Fig. 4 *b*), but higher than the rate of hydrolysis by the γ-less mutant $\alpha_3\beta_3$ of ~5 s^{-1} (27), implying that the short γ-subunits still contribute to the progress of catalysis. The hydrolysis rates of the short-γ mutants above, on the other hand, are higher than the rate of 120° stepping, or three times the average speed, in the bead rotation (Fig. 3). If the infrequent stepping of the mutants compared to the wild-type (Fig. 3 *b*) resulted solely from inefficiency of catalysis in the mutants, e.g., from infrequent ATP binding, then hydrolysis and rotational stepping rates should both be low and of the same value. In fact, the rotation was slower (and unobserved with large beads), which we attribute to the attachment of a bead duplex that would augment the probability of surface hindrance. In the previous study on γ-ΔN4C25 to γ-ΔN22C43, the rotation of 40-nm beads was commensurate with the rate of hydrolysis, whereas 0.29-μm beads rotated more slowly (27).

We note that the activities of the mutants γ-ΔC25 to γ-ΔC36 are almost time-independent, compared with the wild-type that is gradually converted to a steady-state mixture of active and MgADP-inhibited enzymes (Fig. 4 *a*). The mutants might have been inhibited from the beginning, but if we start with inhibited wild-type enzyme, the activity initially rises to reach the same steady-state value. The activities of γ-ΔN4C25 to γ-ΔN22C43 also changed little with time (27), whereas longer mutants up to γ-ΔC21 showed deceleration (26). Leverage action supported by the γ tip may promote the process of inhibition, in addition to allowing rapid rotation to proceed.

Torque of the mutants

Except for the stumblings, the mutants rotated basically in one direction, implying generation of a torque. To infer the torque, we analyzed the instantaneous rotary speed during the 120° stepping, assuming that the speed was limited by viscous friction against the bead duplex. The stepping speed of the short mutants was about half the speed of the wild-type (Fig. 5), implying half the wild-type torque.

For quantitative estimation, we averaged 30 consecutive steps to obtain the thick cyan curves in Fig. 5, and calculated the torque as the slope of the cyan curve (instantaneous rotary speed) times the frictional drag coefficient of the bead duplex, as shown in Eqs. 1 and 2. The wild-type rotated at a constant speed, implying an angle-independent torque of ~40 pN·nm,

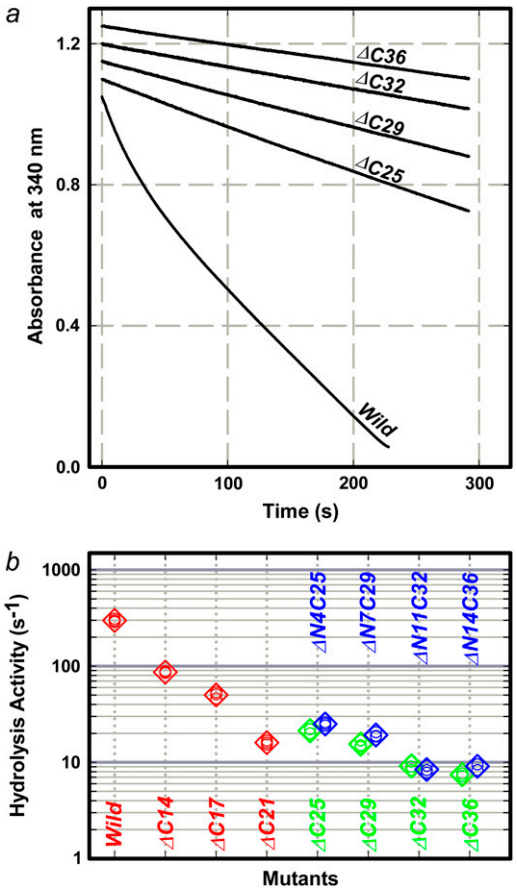

FIGURE 4 ATP hydrolysis activity. (*a*) Time courses of hydrolysis monitored as decrease in NADH absorbance at 340 nm. A decrease of one absorbance unit corresponds to hydrolysis of 1.6×10^{-4} M of ATP. Reaction was initiated by adding F_1 at a final concentration of 10 nM (mutants) or 5 nM (wild-type) to coupled-assay medium containing 2 mM ATP. (*b*) Summary of hydrolysis rates at 2 mM ATP. Green, this work; red, previous work (26), in which mutants were prepared with a regular procedure including heat shock, and bound nucleotides were removed; blue, simultaneous truncation of both N-terminus and C terminus of γ-subunit (27), where treatment with size-exclusion column was performed at room temperature, which helped to stabilize mutants. Small circles indicate individual data, and large diamonds indicate their average.

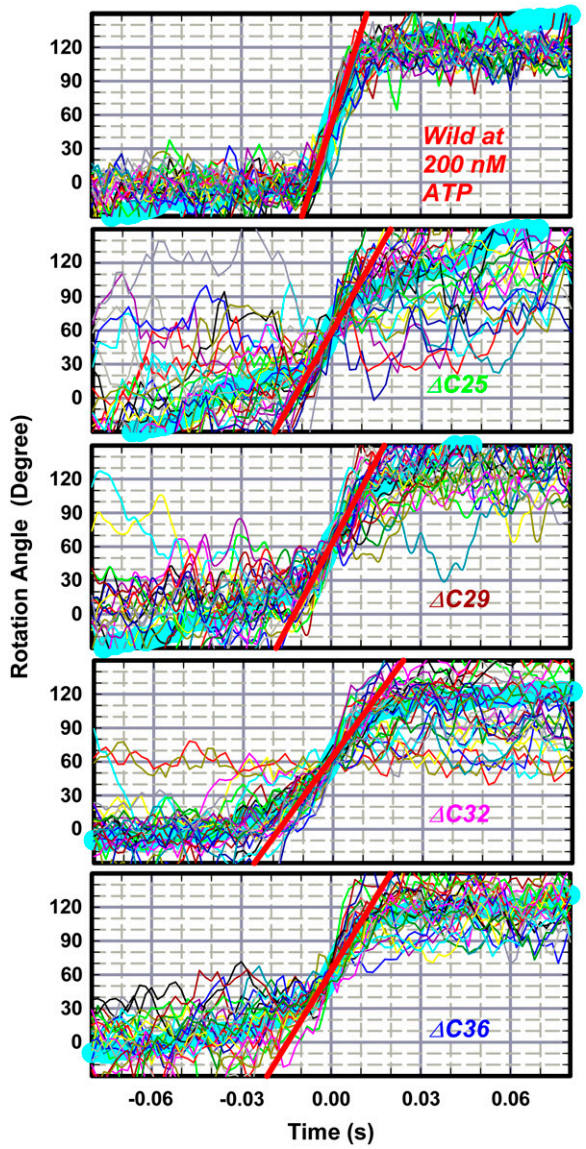

FIGURE 5 Stepping records for torque estimation. Thin colored curves show 30 consecutive steps; thick cyan curve constitutes their average. Individual step records were shifted vertically by a multiple of 120° to obtain overlap. Time zero for each step record was assigned by eye to the data point closest to 60°. Straight red lines indicate linear fit to the cyan curve between 30° and 90°.

as previously reported (7). The torque of the mutants estimated in the central 30°–90° portion of the average curve was ~20 pN·nm (Fig. 6, *green symbols*), half the torque of the wild-type. Angle dependence could not be determined in the mutants because the steps were too noisy. The apparent sluggishness outside the 30°–90° region likely resulted from the simple averaging of noisy and ill-synchronized steps. These mutants, however, apparently produce half the normal torque at least over half the step angle of 120°.

Because the fluctuation of the bead (γ) angle is large in the mutants compared to the wild-type (Fig. 5), one could argue that the 120° steps of the mutants represent occasional large-amplitude thermal fluctuations (diffusion and catch) rather than motion under torque (with overlapping fluctuations). We cannot rule out this possibility completely, but our previous study (26) suggests that our torque estimation is reasonable. There, we used the same method to estimate the torque of the wild-type and mutants γ-ΔC14 to γ-ΔC21 (Fig. 6, *red*). The torque values of these mutants were independent of the ATP concentration between 2 mM and 20 nM. At a saturating concentration of 2 mM ATP, the previous mutants rotated continuously with only occasional stumblings, and thus the torque values at 2 mM ATP, essentially calculated from the average speed over many revolutions, are genuine. At low ATP concentrations, both the wild-type and the mutants rotated in 120° steps, and the fluctuations of γ-ΔC17 and γ-ΔC21 were as extensive as the present mutants of

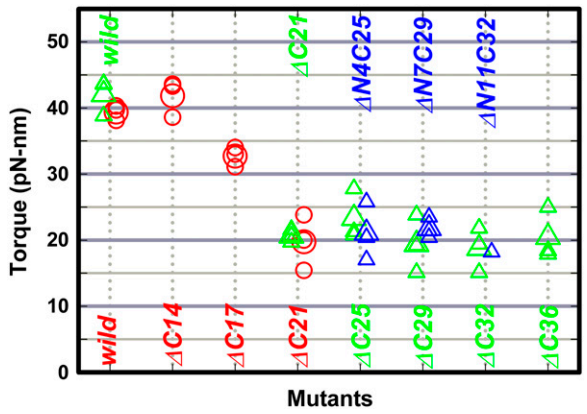

FIGURE 6 Torque of gamma deletion mutants. Green, this study; red (26) and blue (27), previous results. Circles, torque estimated with a duplex of 0.49-μm beads; triangles, 0.29-μm bead duplex. Small symbols represent individual estimations, and large symbols represent their average.

γ-ΔC25 to γ-ΔC36. Yet the torque of stepping and fluctuating γ-ΔC17 and γ-ΔC21 estimated in the 30–90° portion of the averaged steps agreed with the estimates at 2 mM ATP. The apparent torque values for the present mutants are all ~20 pN·nm, similar to the torque of γ-ΔC21. The extent of fluctuations, which, to some extent, varies from bead to bead, is not different from that of the previous mutants. We thus think that the torque values in Fig. 6 are reliable. Thus the residues between γ-ΔC21 and γ-ΔC36 do not contribute to torque production, except for a probable role as lever for an additional torque when the γ tip is present.

DISCUSSION

In the MF_1 structure (Fig. 1 *a*), we see that the α-helical coiled coil of the N-terminus and C- terminus of the γ-subunit deeply penetrates the central cavity of the $\alpha_3\beta_3$ cylinder, to serve as the axle. The axle is held by the cylinder wall at two positions, at the orifice and at the bottom. Presumably, similar contacts/interactions exist in EF_1 and TF_1, as indicated by structural (18,34) and sequence (Fig. 1 *c*) resemblances. Most of the bottom interactions are in the region deleted in the γ-ΔC21 mutation (Fig. 1 *a*, *gray*). Fig. 6 shows that the bottom interactions are essential for the generation of normal torque. Half the torque, however, is produced without the bottom contacts. The middle portion of the axle, i.e., those residues of γ in the central cavity of the $\alpha_3\beta_3$ cylinder, appears to play no positive role in torque production.

The previous study, where both the N-terminus and C-terminus of the γ-subunit were truncated simultaneously (27), indicated nonessential roles for the middle portion. A possibility remained, however, that the tip of the truncated axle still touched the cylinder wall, thereby sustaining the residual torque. Here, we truncated only the C-terminus, leaving the N-terminal helix intact. The results are basically indistinguishable from those of double truncations (Figs. 4 *b* and 6). The implication is that the N-terminal helix alone does not add anything to the mechanism of torque production. Either the remaining N-terminus is too flexible, possibly failing to form a complete α-helix, or its tip remains in the cavity and does not make significant contact with the wall. The residual torque of ~20 pN·nm appears to be produced entirely by the contacts at the orifice.

The rate of ATP hydrolysis (Fig. 4 *b*), which would correspond to the rate of unloaded rotation, also suggests that the middle portion of the axle does not play a significant role in the progression of catalysis. The N-terminus which remained intact in this study does not accelerate catalysis, implying that it cannot lower the energy barrier that causes the stepping behavior at the saturating ATP concentration. Although the measured rate of hydrolysis is not reliable, indicative only of the lower bound, it seems reasonable that the truncated tip that would stay in the central cavity does not play a significant role. For CF_1, a report indicated that truncation of the N-terminal helix alone diminishes ATPase activity, depending on the extent of truncation (35). Whether the lower activity resulted from a lower stability of the reconstituted $\alpha_3\beta_3\gamma$ complex, or from less efficient transmission of the conformational signal to the catalytic sites, has not been established. In this regard, we also note that successive truncations of TF_1 γ, whether both N-terminus and C-terminus or C-terminus alone, resulted in a gradual and significant loss of stability of the complex. The residues in the middle portion of the axle contributed to stability, though not much to function.

The major issue to be clarified is of how the orifice interactions alone can produce the sizable torque. More mysterious is the fact that the γ head alone, the portion of γ that would simply sit on the concave entrance of the orifice, can rotate in the correct direction for more than 100 revolutions without being detached from the stator cylinder (27). We cannot yet propose a persuasive mechanism. New atomic structures, other than those available to date that are not grossly different from each other, are highly awaited. Whether the truncated constructs can synthesize ATP when rotated in reverse is another key question that remains open.

As a final remark, we note that all the γ-truncation studies reported so far, including our own, do not reveal a specific residue in the axle that plays a key role in catalysis or rotation. All show a progressive diminishment of function with degree of truncation, including a plateau phase, as in our studies. Specific interactions, such as the hydrogen bond or salt-bridge formation, appear to play a minor role, if any, in rotation.

We thank R. Shimo-Kon, K. Shiroguchi, T. Okamoto, Y. Onoue, M. Yusuf Ali, D. Patra, and M. Shio for technical assistance and discussions, and K. Sakamaki and M. Fukatsu for encouragement and laboratory management.

This work was supported by a grant-in-aid for Specially Promoted Research and the 21st Century COE Program from the Ministry of Education, Culture, Sports, Science, and Technology of Japan.

REFERENCES

1. Kagawa, Y., and E. Racker. 1966. Partial resolution of the enzymes catalyzing oxidative phosphorylation. IX. Reconstruction of oligomycin-sensitive adenosine triphosphatase. *J. Biol. Chem.* 241:2467–2474.
2. Catteral, W. A., and P. L. Pedersen. 1971. Adenosine triphosphatase from rat liver mitochondria. I. Purification, homogeneity, and physical properties. *J. Biol. Chem.* 246:4987–4994.
3. Cox, G. B., J. A. Downie, L. Langman, A. E. Senior, G. Ash, D. R. H. Fayle, and F. Gibson. 1981. Assembly of the adenosine triphosphatase complex in *Escherichia coli*: assembly of F_0 is dependent on the formation of specific F_1 subunits. *J. Bacteriol.* 148:30–42.
4. Yoshida, M., E. Muneyuki, and T. Hisabori. 2001. ATP synthase—a marvelous rotary engine of the cell. *Nat. Rev. Mol. Cell Biol.* 2:669–677.
5. Boyer, P. D., and W. E. Kohlbrenner. 1981. The present status of the binding-change mechanism and its relation to ATP formation by chloroplasts. *In* Energy Coupling in Photosynthesis. B. R. Selman and S. Selman-Reimer, editors. Elsevier, Amsterdam, The Netherlands. 231–240.
6. Oosawa, F., and S. Hayashi. 1986. The loose coupling mechanism in molecular machines of living cells. *Adv. Biophys.* 22:151–183.
7. Kinosita, K., Jr., K. Adachi, and H. Itoh. 2004. Rotation of F_1-ATPase: how an ATP-driven molecular machine may work. *Annu. Rev. Biophys. Biomol. Struct.* 33:245–268.
8. Abrahams, J. P., A. G. W. Leslie, R. Lutter, and J. E. Walker. 1994. Structure at 2.8 Å resolution of F_1-ATPase from bovine heart mitochondria. *Nature.* 370:621–628.
9. Jault, J.-M., C. Dou, N. B. Grodsky, T. Matsui, M. Yoshida, and W. S. Allison. 1996. The $\alpha_3\beta_3\gamma$ subcomplex of the F_1-ATPase from the thermophilic *Bacillus* PS3 with the βT165S substitution does not entrap inhibitory MgADP in a catalytic site during turnover. *J. Biol. Chem.* 271:28818–28824.
10. Matsui, T., E. Muneyuki, M. Honda, W. S. Allison, C. Dou, and M. Yoshida. 1997. Catalytic activity of the $\alpha_3\beta_3\gamma$ complex of F_1-ATPase without noncatalytic nucleotide binding site. *J. Biol. Chem.* 272:8215–8221.
11. Hirono-Hara, Y., H. Noji, M. Nishiura, E. Muneyuki, K. Y. Hara, R. Yasuda, K. Kinosita Jr., and M. Yoshida. 2001. Pause and rotation of F_1-ATPase during catalysis. *Proc. Natl. Acad. Sci. USA.* 98:13649–13654.
12. Noji, H., R. Yasuda, M. Yoshida, and K. Kinosita Jr. 1997. Direct observation of the rotation of F_1-ATPase. *Nature.* 386:299–302.
13. Yasuda, R., H. Noji, K. Kinosita Jr., and M. Yoshida. 1998. F_1-ATPase is a highly efficient molecular motor that rotates with discrete 120° steps. *Cell.* 93:1117–1124.
14. Adachi, K., R. Yasuda, H. Noji, H. Itoh, Y. Harada, M. Yoshida, and K. Kinosita Jr. 2000. Stepping rotation of F_1-ATPase visualized through angle-resolved single-fluorophore imaging. *Proc. Natl. Acad. Sci. USA.* 97:7243–7247.
15. Yasuda, R., H. Noji, M. Yoshida, K. Kinosita Jr., and H. Itoh. 2001. Resolution of distinct rotational substeps by submillisecond kinetic analysis of F_1-ATPase. *Nature.* 410:898–904.
16. Adachi, K., K. Oiwa, T. Nishizaka, S. Furuike, H. Noji, H. Itoh, M. Yoshida, and K. Kinosita Jr. 2007. Coupling of rotation and catalysis in F_1-ATPase revealed by single-molecule imaging and manipulation. *Cell.* 130:309–321.
17. Shimabukuro, K., R. Yasuda, E. Muneyuki, K. Y. Hara, K. Kinosita Jr., and M. Yoshida. 2003. Catalysis and rotation of F_1 motor: cleavage of ATP at the catalytic site occurs in 1 ms before 40° substep rotation. *Proc. Natl. Acad. Sci. USA.* 100:14731–14736.
18. Shirakihara, Y., A. G. W. Leslie, J. P. Abrahams, J. E. Walker, T. Ueda, Y. Sekimoto, M. Kambara, K. Saika, Y. Kagawa, and M. Yoshida. 1997. The crystal structure of the nucleotide-free $\alpha_3\beta_3$ subcomplex of F_1-ATPase from the thermophilic *Bacillus* PS3 is a symmetric trimer. *Structure.* 5:825–836.
19. Nishizaka, T., K. Oiwa, H. Noji, S. Kimura, E. Muneyuki, M. Yoshida, and K. Kinosita Jr. 2004. Chemomechanical coupling in F_1-ATPase revealed by simultaneous observation of nucleotide kinetics and rotation. *Nat. Struct. Mol. Biol.* 11:142–148.
20. Itoh, H., A. Takahashi, K. Adachi, H. Noji, R. Yasuda, M. Yoshida, and K. Kinosita Jr. 2004. Mechanically driven ATP synthesis by F_1-ATPase. *Nature.* 427:465–468.
21. Wang, H., and G. Oster. 1998. Energy transduction in the F_1 motor of ATP synthase. *Nature.* 396:279–282.
22. Gibbons, C., M. G. Montgomery, A. G. W. Leslie, and J. E. Walker. 2000. The structure of the central stalk in bovine F_1-ATPase at 2.4 Å resolution. *Nat. Struct. Biol.* 7:1055–1061.
23. Iwamoto, A., J. Miki, M. Maeda, and M. Futai. 1990. H^+-ATPase γ subunit of *Escherichia coli*: role of the conserved carboxyl-terminal region. *J. Biol. Chem.* 265:5043–5048.
24. Sokolov, M., L. Lu, W. Tucker, F. Gao, P. A. Gegenheimer, and M. L. Richter. 1999. The 20 C-terminal amino acid residues of the chloroplast ATP synthase γ subunit are not essential for activity. *J. Biol. Chem.* 274:13824–13829.
25. Müller, M., O. Pänke, W. Junge, and S. Engelbrecht. 2002. F_1-ATPase, the C-terminal end of subunit γ is not required for ATP hydrolysis driven rotation. *J. Biol. Chem.* 277:23308–23313.
26. Hossain, M. D., S. Furuike, Y. Maki, K. Adachi, M. Y. Ali, M. Huq, H. Itoh, M. Yoshida, and K. Kinosita Jr. 2006. The rotor tip inside a bearing of a thermophilic F_1-ATPase is dispensable for torque generation. *Biophys. J.* 90:4195–4203.
27. Furuike, S., M. D. Hossain, Y. Maki, K. Adachi, T. Suzuki, A. Kohori, H. Itoh, M. Yoshida, and K. Kinosita Jr. 2008. Axle-less F_1-ATPase rotates in the correct direction. *Science.* 319:955–958.
28. Matsui, T., and M. Yoshida. 1995. Expression of the wild-type and the Cys-/Trp-less $\alpha_3\beta_3\gamma$ complex of thermophilic F_1-ATPase in *Escherichia coli*. *Biochim. Biophys. Acta.* 1231:139–146.
29. Monticello, R. A., E. Angov, and W. S. A. Brusilow. 1992. Effects of inducing expression of cloned genes for the F_0 proton channel of the *Escherichia coli* F_1F_0 ATPase. *J. Bacteriol.* 174:3370–3376.
30. Ohta, S., M. Yohda, M. Ishizuka, H. Hirata, T. Hamamoto, Y. Otawara-Hamamoto, K. Matsuda, and Y. Kagawa. 1988. Sequence and over-expression of subunits of adenosine triphosphate synthase in thermophilic bacterium PS3. *Biochim. Biophys. Acta.* 933:141–155.
31. Adachi, K., H. Noji, and K. Kinosita Jr. 2003. Single molecule imaging of the rotation of F_1-ATPase. *Methods Enzymol.* 361B:211–227.
32. Sakaki, N., R. Shimo-Kon, K. Adachi, H. Itoh, S. Furuike, E. Muneyuki, M. Yoshida, and K. Kinosita Jr. 2005. One rotary mechanism for F_1-ATPase over ATP concentrations from millimolar down to nanomolar. *Biophys. J.* 88:2047–2056.
33. Pänke, O., D. A. Cherepanov, K. Gumbiowski, S. Engelbrecht, and W. Junge. 2001. Visco-elastic dynamics of actin filaments coupled to rotary F-ATPase: angular torque profile of the enzyme. *Biophys. J.* 81:1220–1233.
34. Hausrath, A. C., R. A. Capaldi, and B. W. Matthews. 2001. The conformation of the ε- and γ-subunits within the *Escherichia coli* F_1 ATPase. *J. Biol. Chem.* 276:47227–47232.
35. Ni, Z.-L., H. Dong, and J.-M. Wei. 2005. N-terminal deletion of the γ subunit affects the stabilization and activity of chloroplast ATP synthase. *FEBS J.* 272:1379–1385.
36. Walker, J. E., I. M. Fearnley, N. J. Gay, B. W. Gibson, F. D. Northrop, S. J. Powell, M. J. Runswick, M. Saraste, and V. L. J. Tybulewicz. 1985. Primary structure and subunit stoichiometry of F_1-ATPase from bovine mitochondria. *J. Mol. Biol.* 184:677–701.